

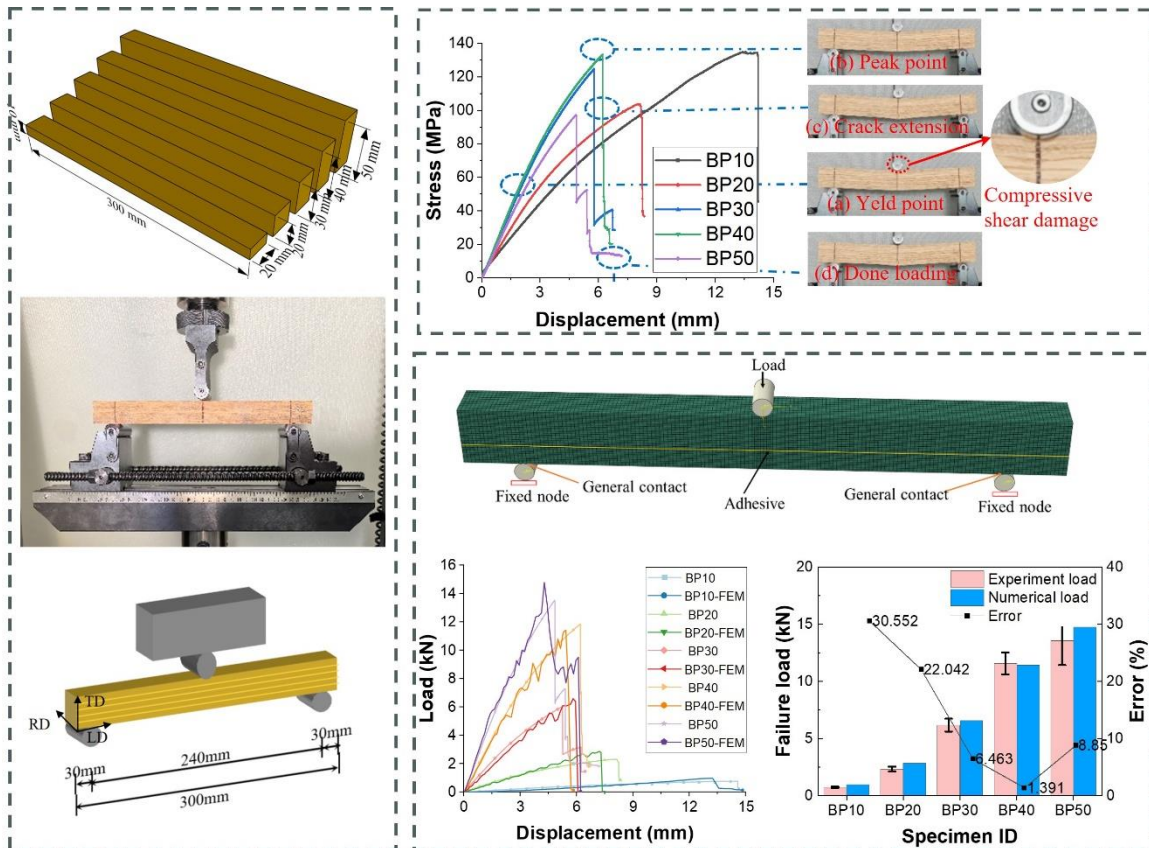
# Influence of Strand Size on the Bending Properties of Parallel Strand Bamboo

Wenli Zhu,<sup>a,b</sup> Jiannan Zhou,<sup>c</sup> Guo Chen,<sup>a,b,\*</sup> and Zhenyu Qiu<sup>a,\*</sup>

\*Corresponding authors: [chenguo@njfu.edu.cn](mailto:chenguo@njfu.edu.cn) (G Chen); [qzy@njfu.edu.cn](mailto:qzy@njfu.edu.cn) (ZY Qiu)

DOI: 10.15376/biores.20.1.1691-1702

## GRAPHICAL ABSTRACT



# Influence of Strand Size on the Bending Properties of Parallel Strand Bamboo

Wenli Zhu,<sup>a,b</sup> Jiannan Zhou,<sup>c</sup> Guo Chen,<sup>a,b,\*</sup> and Zhenyu Qiu<sup>a,\*</sup>

Most bamboo composites are designed referring to the specifications of wood structures. However, this approach is inadequate due to the volume difference between bamboo bundles and other fibers. Previous studies have investigated the effects of strand size of parallel strand bamboo (PSB) in tension and compression. Here, to investigate the impact of varying span-height ratio on the flexural characteristics of PSB, specimens with five different section heights were designed. Numerical simulations were performed to reveal the deformation, the failure process, and the load carrying ability of the PSB beams. The first-order anisotropic beam theory was applied to predict the internal forces. The results show that the bending property of the PSB is closely related to the section height. It is recommended that the dimension of length × width × height (300 mm × 20 mm × 30 mm) should be the most appropriate specimen size for the bending experiment. The error between the theoretical value and the test value was only about 0.4%. These endeavors can facilitate the establishment of bending test standards for bamboo structures.

DOI: 10.15376/biores.20.1.1691-1702

Keywords: Parallel strand bamboo; Bending property; Size effect; Span-height ratio; Numerical analysis

Contact information: a: College of Civil Engineering, Nanjing Forestry University, Nanjing 210037, China; b: Jiangsu Carbon Sequestration Materials and Structural Technology of Bamboo & Wood Research Center, Nanjing Forestry University, Nanjing 210037, China; c: State Key Laboratory for Disaster Prevention & Mitigation of Explosion & Impact, Army Engineering University of PLA, Nanjing 210007, China; \*Corresponding authors: chenguo@njfu.edu.cn (G Chen); qzy@njfu.edu.cn (ZY Qiu)

## INTRODUCTION

With the continuous promotion of green building materials in recent years, wood and bamboo are gradually being applied to practical projects as new building materials (Ugalde *et al.* 2021). The field of wood structure research has developed a comprehensive framework that encompasses the examination of material properties, theoretical modeling (Cabral and Blanchet 2021), connection behaviors (Zhang *et al.* 2023; Zhang *et al.* 2024), and the establishment of standard specifications. Compared to the lack of wood resources, China contains rich bamboo resources (Goh *et al.* 2020). Due to the fast growth cycle, bamboo has been an important resource for the development of green building (Sharma *et al.* 2015).

Parallel strand bamboo (PSB), as an environmentally friendly and high-performance engineered bamboo material (Wegst *et al.* 2015) that holds vast potential for application. Numerous scholars from both domestic and international contexts have conducted extensive research on its thermal, aging and other mechanical properties (Xu *et al.* 2017; Cui *et al.* 2024; Huang *et al.* 2024; Li *et al.* 2024; Deng *et al.* 2024a,b, Yang *et al.* 2024; Xue *et al.* 2024). Under the background of vigorously developing the bamboo industry in China, PSB will become a powerful support material to realize green development.

With the increased resin content and density of PSB, the bending strength and modulus have been shown to increase (Zhao *et al.* 2019; Sun *et al.* 2020). In recent years, researchers have investigated the bending properties of PSB, including physical or mechanical properties and theories. In the field of engineering, bamboo beams have emerged as a sustainable and cost-effective alternative to traditional wooden beams. A new type of large-span reinforced bamboo scrimber composite beam was designed to study the bending properties. Six types of beams with a dimension of length  $\times$  width  $\times$  height (3600 mm  $\times$  150 mm  $\times$  150 mm), were used for bending tests (Zhong *et al.* 2017). In the examination of the fundamental flexural characteristics of PSB, the bending properties of bamboo scrimber with different hole sizes and positions were investigated (Zhao *et al.* 2019). The testing samples with dimensions of 330 mm  $\times$  38 mm  $\times$  17 mm (Length  $\times$  Height  $\times$  Width) were designed according to Chinese National Standards GB/T 1928 (2009) and GB/T 28993 (2012). To explore the anisotropic behavior of PSB, seven kinds of PSB beams with different fiber orientations were tested (Qiu *et al.* 2020). The impact bending behaviors of them were also discussed (Qiu *et al.* 2021). Furthermore, the low velocity flexural impact behaviors of bamboo fiber reinforced composite beams were investigated (Qiu *et al.* 2021). The dimension of all specimens in these articles was 300 mm  $\times$  20 mm  $\times$  20 mm. To elucidate the bending failure mechanism of bamboo scrimber, natural bamboo (NB) served as the benchmark for comparative analysis. The specimens with the dimension of 160 mm (longitudinal)  $\times$  10 mm (radial)  $\times$  10 mm were manufactured and subjected to four-point bending tests (Wang *et al.* 2022). A sample dimension of the support span was selected, measuring 100 mm (length) and the thickness was 10 mm of the bending part, to investigate the bending properties of bamboo scrimber, and the impact of varying loading rates and pre-tension on these properties was examined (Guan *et al.* 2023).

Other than the abovementioned research, no standard specimen specification for bamboo composite test has been specified. Researchers usually refer to the existing research specifications of wood, such as GB/T50329 (2012) and ASTM D143 (2014). However, due to the particularity of the production process, the PSB is made by hot pressing, and the unit volume of the bamboo strands is much greater than that of the bamboo fibers. The size design of PSB specimen in accordance with the wood structure specification could not represent its performance well, which had been verified in tension and compression (Zhu *et al.* 2022). Therefore, the density of specimen has a great influence on the performance of specimen. It remains to be investigated whether the dimensions of the bending specimen can accurately represent the standard bending test for bamboo composites by solely referencing the standard bending test size of wood or composite materials in the bending test standards, considering that each bamboo strand has a characteristic size at the millimeter level. Thus, it is necessary to study the size effect of PSB in bending for the standard of bamboo composite specified in the future.

To explore the size effect of the basic bending properties and verify whether the wood structure test standard and the composite test standard can be applied to the PSB, PSB specimens with different sizes were prepared. Considering the diversity of size combinations and the limitation of content, the size effect was considered only from the perspective of different span-height ratios, and their bending properties were tested.

## EXPERIMENTAL

### Material and Specimen

PSB is a type of unidirectional bamboo fiber-reinforced composite material made from original bamboo filament bundles or fibrous veneer. The production process is as follows: The culm of 3 to 5 years old *Phyllostachys pubescens* was cut into bamboo slices that were crushed and fluffed into bamboo fiber bundles. The crushed bamboo fiber bundles were then treated with saturated steam to be carbonized before they were dried and immersed in phenol formaldehyde resin. Subsequently, the resin saturated bamboo fiber bundles were reorganized unidirectionally in a mold and hot-pressed into the final bamboo scrimber products.

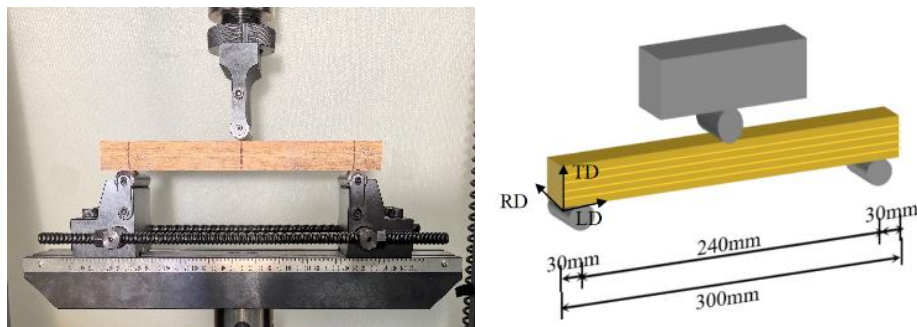


**Fig. 1.** The diagram of experiment device

The specimens were cut from the PSB plate, produced by Hunan Taohuajiang Bamboo Technology Co., Ltd. They were conditioned under  $20 \pm 5$  °C temperature and  $60 \pm 5\%$  relative humidity conditions in an airconditioned room. The average density was  $1.178 \text{ g/cm}^3$ . The specimens were tested according to the corresponding standards of the wood bending strength test method (GB / T1936.1-2009). The size design of the specimens for the bending strength of PSB was initially determined to be 300 mm (length)  $\times$  20 mm (width)  $\times$  20 mm (height), and the effective length was 240 mm. In this study, to investigate the effect of varying height-to-width ratios on the bending properties of specimens, the length (300 mm) and width (20 mm) of the specimen remain constant, the cross-sectional thickness of specimens parallel to grain were gradually increased, with changes from 10 mm to 50 mm, at 10 mm intervals. Each group had 20 specimens, with a total of 100. The specimen groups were BP10, BP20, BP30, BP40, and BP50, where B represents bending test and P represents the specimen parallel to the grain. The number indicates the different sizes of the section height, such as 10 represents the section height of the specimen is 10 mm. A diagram of specimen size design and experimental loading device is shown in Fig. 1. The test instrument was an LD26 series microcomputer controlled electronic universal testing machine, manufactured by LISHI (Shanghai) instrument Co., Ltd., China. The specimens were loaded with a loading rate of 2 mm/min until the specimen failed.

### Failure Analysis

The failure mode of the PSB bending test associated with the stress-displacement curves and data was analyzed. In this test, the failure mode of all specimens showed mid-span fracture. At the initial stage of bending loading, the stress-displacement curve was linear, and the specimen had no obvious deformation. As the load increased, the deformation gradually increased. In BP10 to BP30, when the specimen reached the

ultimate bearing capacity, the specimen made a brittle sound, and cracks appeared at the bottom of the mid-span of the specimen. At the later stage of bending load loading, the tensile area below the neutral axis of the specimen continued to break, and the cracks began to expand from the bottom to the side. After the cessation of loading, the specimen exhibited a high degree of resilience. However, there was a little difference in BP40 and BP50. The initial damage was observed surrounding the indenter when entering the nonlinear stage, characterized by a minor compressive shear failure. Then, the cracks appeared at the bottom of the beam and expanded upward with the increase of load. The observed phenomenon was primarily attributed to the distribution of bending stress, shear stress, and the alignment of fibers. As the sectional height increases, it became more susceptible to initial damage within the compression zone. The bending deformation of the specimen continued to increase until the specimen was destroyed, and the specimen failed to exhibit satisfactory resilience when the loading was stopped. The failure patterns of specimen across four distinct stages: (a) yield point, (b) peak point, (c) crack extension, and (d) done loading; are illustrated in Fig. 2(c) and (d).

## EXPERIMENTAL RESULTS

### Three-point Bending

The reliability and discreteness of the measured 100 sets of data were analyzed. According to mechanical theory of materials, the bending strength ( $\sigma_{bw}$ ) and the modulus ( $E_{bw}$ ) of specimens can be calculated by Eqs. (1) and (2). The specific information on the basic bending properties is listed in Table 1, which are given the average value with the standard deviation in parentheses,

$$\sigma_{bw} = \frac{3P_{max}l}{2bh^2} \quad (1)$$

where  $P_{max}$  is the maximum bearing capacity measured by the test (N);  $l$  is the effective length of the specimen (mm), and the value is 240 mm;  $b$  is the width of the bending specimen (mm); and  $h$  is the height of the bending specimen (mm),

$$E_{bw} = \frac{\Delta Pl^3}{4bh^3\Delta f} \quad (2)$$

where,  $\Delta P$  is the load increment in the elastic linear stage of the specimen (N); and  $\Delta f$  is the deflection increment of the elastic linear stage of the specimen (mm).

**Table 1.** The Results of Bending Test

Group (b*h; mm)	$P_{max}$ (kN)	$\Delta m$ (mm)	$\sigma_{bw}$ (MPa)	$E_{bw}$ (GPa)
BP10 (20*10)	0.743 (0.077)	13.595 (1.932)	133.704 (13.869)	13.209 (2.083)
BP20 (20*20)	2.341 (0.208)	8.258 (0.638)	105.330 (9.339)	8.725 (0.717)
BP30 (20*30)	6.174 (0.565)	5.490 (0.716)	123.48 (11.304)	8.501 (0.759)
BP40 (20*40)	11.573 (0.970)	6.115 (0.690)	130.192 (10.911)	6.261 (0.443)
BP50 (20*50)	13.559 (2.142)	5.258 (1.268)	97.623 (15.425)	4.614 (0.398)

Note:  $\Delta m$  represents the displacement at the peak point.

It is clear that the ultimate bearing capacity of the specimen increased with the height of the section, whereas the bending modulus decreased as the section height increased.

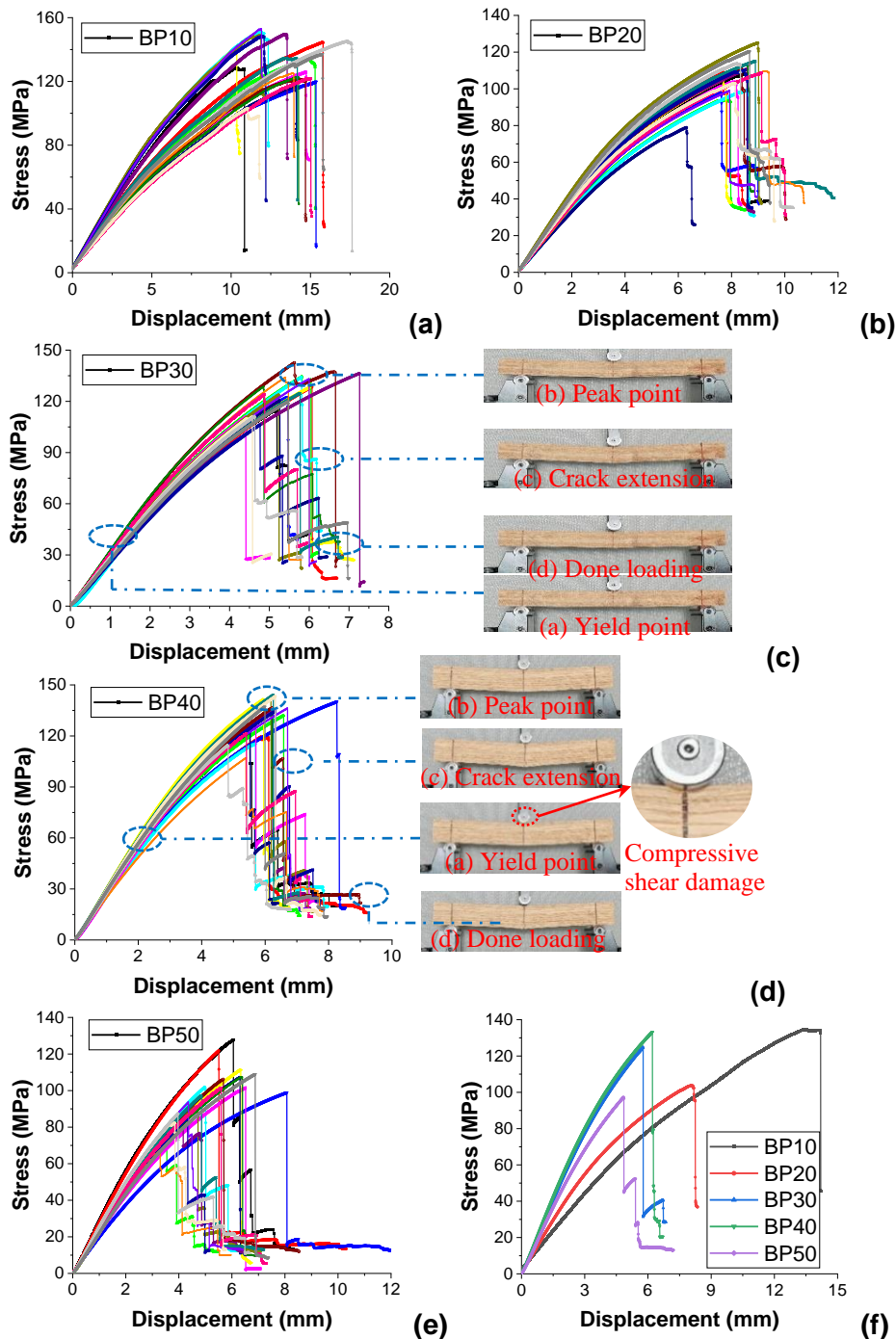


**Fig. 2.** The stress-displacement curves and failure modes of different flexural groups (a) through (e), and the comparison of typical stress-displacement curves (f)

This was probably because a higher section height results in a more unstable specimen. The deflection of the specimen with a section height of 10 mm was heavy during the bending process, which exceeded the section height of the specimen. It did not meet the small deformation assumption in material mechanics, so the calculation values were quite different. In future research, the large deformation theory will be considered to analyze it, and it will not be compared with other results. According to the results presented in Table 1, specimens with a width of 20 mm and a cross-section height of 20 mm

demonstrated superior bending modulus, which was similar to specimens with a width of 20 mm and a cross-section height of 30 mm. Conversely, those with a cross-section height of 40 mm exhibited enhanced bending strength.

### Stress-displacement Curves

The bending stress-displacement curves of PSB in three-point bending are demonstrated in Fig. 2 (a through e), which can be characterized by three distinct phases: elastic, elastic-plastic, and failure. With the increase of section height, the cracks appeared at the bottom of the specimen, after extending to the side surface. Due to the increase of section height, the height of the tensile zone of the specimen became larger. The specimen could still bear a certain load until the cracks in the side tensile zone expanded rapidly and the specimen became completely destroyed.

Figure 2 (f) shows the comparison of typical stress-displacement curves in each group. It can be clearly seen that with the increase of section height, the deflection of the specimen gradually decreased, the instability gradually increased, and the force had an obvious steep dropping trend. The larger the section height, the more obvious was the steep drop. This means that the bending failure was more brittle with the increasing section height.

The stress loss due to the propagation of cracks in each set of specimens was examined. It was observed that as the height increased, the residual stress diminished progressively. Specifically, BP20 exhibited a stress loss of approximately 45%, BP30 about 55%, BP40 around 65%, and BP50 roughly 70%. This implies that both BP40 and BP50 exhibited a more pronounced brittleness during the failure process.

### Comparison

The bending strength and modulus of elasticity to different flexural groups are shown in Fig. 3. The orange bar graph represents the mean values for each group, whereas the green bar graph illustrates the characteristic values for each group. Clearly the bending strength and modulus of group BP10 were quite different from others. BP10 was mostly like a one-way plate rather than a beam. Thus, results related to that specimen will not be discussed in this paper.

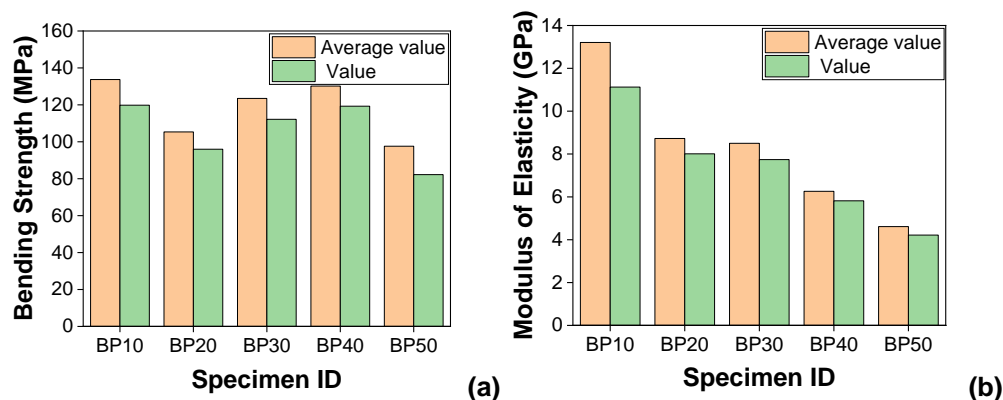


Fig. 3. The bending strength (a) and modulus of elasticity to different flexural groups (b)

It is apparent that BP30 and BP40 exhibited comparable bending strengths, with BP40's bending strength surpassing that of BP30 approximately 6.3%. Conversely, the bending modulus of BP30 exceeded that of BP40 by roughly 38.2%. In the remaining four groups, as depicted in Fig. 3(b), it is evident that BP30 possessed a similar bending

modulus to BP20, which diminished with an increase in section height.

Based on the comparisons presented and the observed performance of each specimen group throughout the testing process, the BP30 showed higher bending strength than BP20, while the modulus was higher than BP40 and BP50. Although BP40 exhibited the highest bending strength, it was prone to initial failure in the compression zone during the fracture process. Thus, it is recommended that the specimen with a section height of 30 mm and a width of 20 mm can be taken in the basic bending mechanical experiments.

## FINITE ELEMENT MODELLING

### Modeling and Properties of the Bamboo Composite Beam

The numerical simulations were conducted using Abaqus/Explicit (Dassault SIMULIA, 2020, Providence, RI, USA). A three-dimensional deformable composite beam of  $300 \times 20 \times 10$  (20/30/40/50) mm was modeled in ABAQUS to perform the simulation. Three steel cylinders with a diameter of 20 mm were modeled to perform the three-point bending test on PSB beam. The PSB beam and the indenter were modeled as shown in Fig. 4. The element type was 8-node linear brick (C3D8R). A region of fine mesh ( $1 \text{ mm} \times 1 \text{ mm}$ ) was considered near the middle indenter/PSB beam contact region, and a coarser mesh ( $2 \text{ mm} \times 1 \text{ mm}$ ) was used in the outer regions to improve the computational efficiency. The contact between the indenter and the PSB beam was defined as general contact. The friction coefficient of the contact was 0.3.

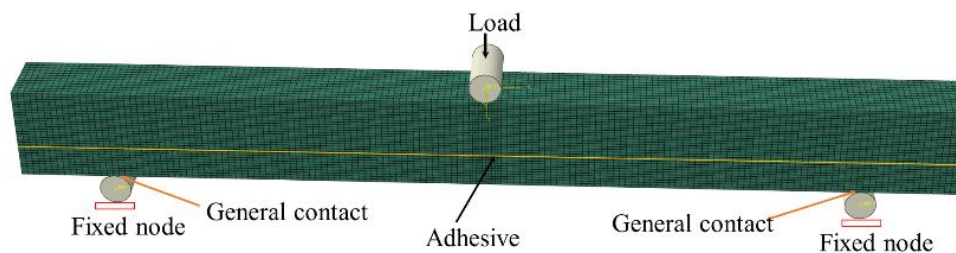


Fig. 4. Finite element model and boundary conditions for BP30

The 3D Hashin damage model was applied to perform the beam using a user-defined material model. It is desirable to use the Hashin criterion to estimate the damage mode of multiple stress components of the composite materials (Gorrepotu *et al.* 2021). The damage to the composites mainly occurs in the form of matrix cracking, fiber breaking, and delamination. Hashin criteria are preferred to estimate the damage modes on the composites by more than one stress component. This criterion is specifically used to predict the damage in unidirectional fiber-reinforced composites.

In the experiment, the phenomenon of delamination cracking in some height bamboo beams was observed. To better describe the stratified failure phenomenon, the cohesive zone model was introduced into the finite element model. Cohesive element behavior is generally characterized by a traction separation law, which shows the relation between the traction and separation in the cohesive element (Truong *et al.* 2019). Three-dimensional cohesive elements (COH3D8) were selected to represent the behavior of the cohesive zone model.

## Numerical Results and Discussion

As shown in Fig. 5, several damage mechanisms were observed in the post-mortem analysis of the specimens including matrix cracking, fiber failure, splitting, delamination, and fiber buckling. The failure mechanisms, such as fiber fracture, matrix failure, splitting, and delamination are usually found in specimens with section height below 30 mm. In addition to the aforementioned failure mechanisms, buckling failure occurs if the section height exceeds 30 mm. There are discrepancies between the simulated parameters and the actual specimen, leading to a more pronounced failure phenomenon in simulations. This is attributed to the fact that the specimens are designed with a laminated structure during the simulation process, which results in particularly evident interlayer cracking. In contrast, the actual component is formed through integrated hot pressing, resulting in less noticeable cracking between the transverse layers. Nevertheless, the simulated failure phenomenon closely aligns with the observed behavior during testing.

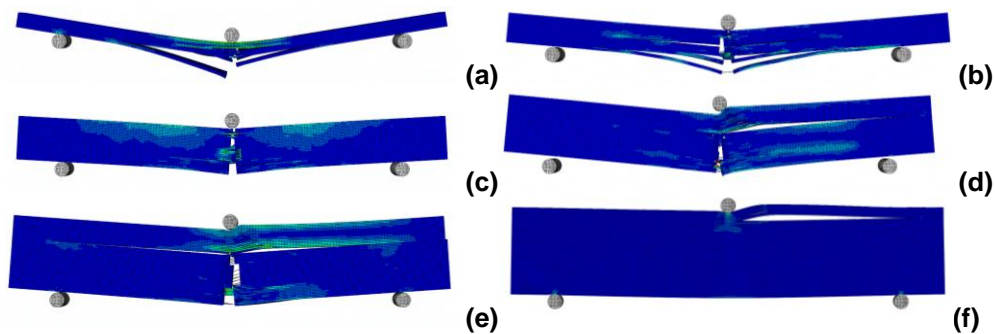


**Fig. 5.** Prediction of failure shape for (a) BP10, (b) BP20, (c) BP30, (d) BP40, (e) BP50, and (f) BP60

Figure 6 (a) compares the predicted failure and those obtained from the experimental data, showing that the simulation curve matched well with the experimental one in terms of slope, peak load, and even displacement in BP30 and BP40. This is consistent with the experimental results; that is, the BP30 and BP40 specimens had the better discreteness.

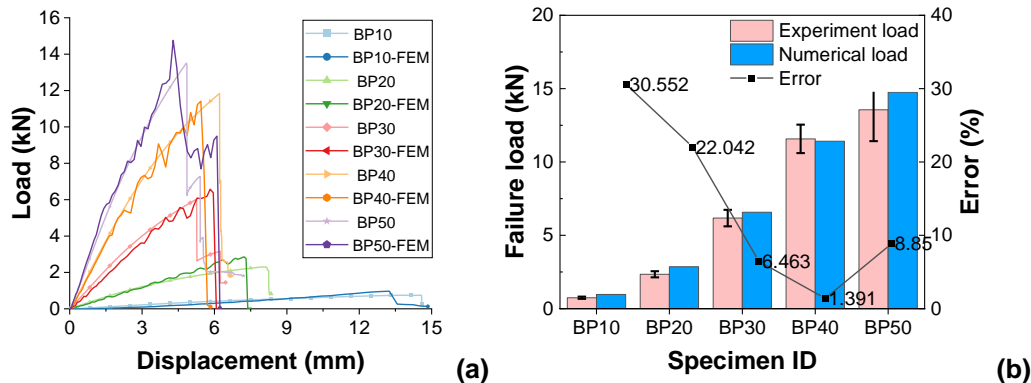


**Fig. 6.** (a) The numerical and experimental failure loads and (b) error of them for all groups

Figure 6(b) illustrates the error in failure load and numerical load for all specimen groups. It is evident that the BP40 exhibited the lowest error value, whereas the BP10 displayed the highest. This is because there are certain defects in the production of the specimen in the factory, and the distribution of bamboo bundles in a single specimen is not

uniform. In the numerical simulation, it is generally considered that the fiber is evenly distributed. Thus, it is reasonable to expect an error between the numerical results and the test results. In the group with lower section height, such as BP20, the load error was also the highest due to the low bamboo bundle content of the specimens and the high possibility of non-uniform distribution. Just as Zhu *et al.* (2022) described for the comparison between bamboo fiber and wood fiber, the test results of basic bending test of PSB simply referring to the size of wood bending standard specimens were quite discrete.

**Table 2.** Comparison of Numerical Values in Different Group

Group	BP10	BP20	BP30	BP40	BP50	BP60
Peak load (kN)	0.970	2.857	6.573	11.412	14.759	14.400
$\sigma_{bw}$ (MPa)	174.60	128.57	131.46	128.39	106.26	72.00
Displacement (mm)	13.244	7.229	5.820	5.433	4.288	3.404

Additionally, the specimen with increased cross-sectional height was anticipated based on numerical simulations, as demonstrated in Fig. 5(f). The dimensions of the specimen were as follows: an effective length of 240 mm, a width of 20 mm, and a height of 60 mm. The simulation results indicate that BP60 fractures initially in the compression zone, leading to the failure of the specimen, while the crack is not formed in the tensile zone. In comparison with BP50, the peak load of the finite element model does not exhibit an obvious increase with the increment in section height, and the bending strength initially increases and then decreases as the section height increases, as shown in Table 2. In contrast, upon reaching the peak load, there is a substantial reduction in displacement, suggesting that the BP60 specimen demonstrates increased brittleness. This also indicates that the load-bearing capacity of the specimen increases with its section height, eventually reaching a stable limit.

### Demonstration of Nonlinear Beam Theory Model

Qiu *et al.* (2020) proposed the first-order anisotropic beam theory based on three-point bending tests of PSB beams with different fiber angles. Based on this theory, the stress state of PSB beam under the ultimate load can be calculated, which were compared with those calculated in test data (Table 1), as listed in Table 3.

**Table 3.** Comparison of Theoretical and Experimental Values in Different Group

Group	$P_{max}$ (kN)	$\sigma_x$ (MPa)	$\tau_{xy}$ (MPa)	$\sigma_{test}$ (MPa)	Error
BP10	0.743	133.198	0.15	133.704	0.38%
BP20	2.341	104.918	0.47	105.330	0.39%
BP30	6.174	122.980	1.23	123.480	0.40%
BP40	11.573	129.669	2.31	130.192	0.40%
BP50	13.559	97.229	2.71	97.623	0.40%

The theoretical value of internal force derived from the first order anisotropic beam theory was compared with the experimental value. The error was only about 0.40%, which further confirms the correctness of the theory.

## CONCLUSIONS

In this study, the following conclusions can be drawn from bending testing, which are of certain importance to the establishment of bamboo structure specifications in China, and the appropriate specimen size for bending is suggested.

1. The bending strength of the PSB specimens is closely associated with their cross-section height. As the height increases, the capacity to bear bending loads may vary, which potentially is due to the distribution of stress across the material's cross-sectional area.
2. The dimension of 300 mm × 20 mm × 30 mm (length × width × height) demonstrated stability in evaluating bending strength and elastic modulus among tested PSB specimens, suggesting that this size leads to reliable and reproducible results for bending properties.
3. The failure modes predicted by the numerical model were consistent with those observed experimentally, reinforcing the model's reliability in predicting not just the load but also the performance in which the specimens fail under stress.
4. The study also determined that the first-order anisotropic beam theory model provided more precise predictions of the bending properties for PSB specimens. The error was only about 0.4%. This finding suggests that the model is a valuable tool for engineers and researchers aiming to accurately forecast the bending behavior of PSB materials during design and analysis phases.

## Declaration of Competing Interest

The authors declare that they have no known competing financial interests or personal relationships that could have appeared to influence the work reported in this paper.

## ACKNOWLEDGEMENTS

Supports from National Natural Science Foundation of China (52178220) is gratefully acknowledged.

## REFERENCES CITED

- ASTM D143-09 (2014). "Standard test method for small clear specimen of timber," ASTM International, West Conshohocken, PA, USA.
- Cabral, M., and Blanchet, P. (2021). "A state of the art of the overall energy efficiency of wood buildings-an overview and future possibilities," *Materials* 14(8), article ID 1848. DOI: 10.3390/ma14081848
- Cui, Z., Xu, M., Shen, Y., and Tu, L. (2024). "The impact of temperature variations on the thermal and charring characteristics of laminated bamboo lumber," *European Journal of Wood and Wood Products* 82, 1159-1169. DOI: 10.1007/s00107-024-02069-z
- Deng, J., Wei, Y., Chen, S., Huang, S., Ding, M., and Li, G. (2024a). "Aging properties of bamboo scrimber after cyclic dry-wet exposure," *Construction and Building*

- Materials* 453, article ID 139043. DOI: 10.1016/j.conbuildmat.2024.139043
- Deng, J., Wei, Y., Yi, J., Chen, J., and Zhang, Z. (2024b). “Flexural properties of bamboo scrimber under different temperature conditions: Experimental study and mathematical model,” *Construction and Building Materials* 445, article ID 137958. DOI: 10.1016/j.conbuildmat.2024.137958
- GB/T 1928-2009 (2009). “General requirements for physical and mechanical tests of wood,” Standardization Administration of China, Beijing, China.
- GB/T 28993 (2012). “Standard test methods for mechanical properties of structural lumber,” Standardization Administration of China, Beijing, China.
- GB/T 50329 (2012). “Standard for test methods of timber structures,” Standardization Administration of China, Beijing, China.
- Goh, Y., Yap, S., and Tong, T. (2020). “Bamboo: The emerging renewable material for sustainable construction,” *Encyclopedia of Renewable and Sustainable Materials 2*, 365-376. DOI: 10.1016/B978-0-12-803581-8.10748-9
- Gorrepotu, S., Kishore, D., and Rabindra, N. (2021). “Finite element analysis of low-velocity impact behavior of green composites,” *Materials Today* 46(2), 1290-1297. DOI: 10.1016/j.matpr.2021.02.130
- Guan, S., Zhao, J., and Dai, L. (2023). “Static and dynamic mechanical behaviors of bamboo scrimber under combined tension-bending,” *Composite Science Technology* 242, article ID 110191. DOI: 10.1016/j.compscitech.2023.110191
- Huang, Y., Xu, M., Zhang, Y., and Cui, Z. (2024). “Experimental study on combustion characteristics of engineered bamboo considering smoldering and self-extinction,” *Industrial Crops and Products* 222(2), article ID 119652. DOI: 10.1016/j.indcrop.2024.119652
- Li, Q., Xu, B., Chen, K., Cui, Z., Liu, Y., and Zhang, L. (2024). “Experimental and three-dimensional numerical investigations of dehydration and pyrolysis in wood under elevated and high temperatures,” *Buildings* 14(6), article 1547. DOI: 10.3390/buildings14061547
- Qiu, Z., Wang, J., and Fan, H. (2021). “Impact bending behaviors of parallel bamboo strand lumber beams: Velocity sensitivity and anisotropy,” *Composite Structure* 263, article ID 113711. DOI: 10.1016/j.compstruct.2021.113711
- Qiu, Z., Wang, J., and Fan, H. (2021). “Low velocity flexural impact behaviors of bamboo fiber reinforced composite beams,” *Polymer Testing* 94, article ID 107047. DOI: 10.1016/j.polymertesting.2020.107047
- Qiu, Z., Wang, J., He, H., and Fan, H. (2020). “First-order anisotropic beam model and failure criterion for flexural parallel bamboo strand lumbars,” *Construction and Building Materials* 263, article ID 120125. DOI: 10.1016/j.conbuildmat.2020.120125
- Sharma, B., Gatóo, A., and Ramage, M. (2015). “Effect of processing methods on the mechanical properties of engineered bamboo,” *Construction and Building Materials* 83, 95-101. DOI: 10.1016/j.conbuildmat.2015.02.048
- Sun, X., He, M., and Li, Z. (2020). “Novel engineered wood and bamboo composites for structural applications: State-of-art of manufacturing technology and mechanical performance evaluation,” *Construction and Building Materials* 249, article ID 118751. DOI: 10.1016/j.conbuildmat.2020.118751
- Truong, V., Kwak, B., Roy, R., and Kweon, J. (2019). “Cohesive zone method for failure analysis of scarf patch-repaired composite laminates under bending load,” *Composite Structure* 222, article ID 110895. DOI: 10.1016/j.compstruct.2019.110895
- Ugalde, D., Almazán, J. L., María, S. H., and Guindos, P. (2019). “Seismic protection

- technologies for timber structures: A review,” *European Journal of Wood and Wood Products* 77, 173-194. DOI: 10.1007/s00107-019-01389-9
- Wang, X., Luo, X., Ren, H., and Zhong, Y. (2022). “Bending failure mechanism of bamboo scrimber,” *Construction and Building Materials* 326, article ID 126892. DOI: 10.1016/j.conbuildmat.2022.126892
- Wegst, U., Bai, H., Saiz, E., Tomsia, A., and Ritchie, R. O. (2015). “Bioinspired structural materials,” *Nature Materials* 14(1), 23-36. DOI: 10.1038/nmat4089
- Xu, M., Cui, Z., Chen, Z., and Xiang, J. (2017). “Experimental study on compressive and tensile properties of a bamboo scrimber at elevated temperatures,” *Construction and Building Materials* 151, 732-741. DOI: 10.1016/j.conbuildmat.2017.06.128
- Xue, X., Li, H., and Rodolfo, L. (2024). “A review of basic mechanical properties of bamboo scrimber based on small-scale specimens,” *Journal of Renewable Materials* 12(4), 869-894. DOI: 10.32604/jrm.2024.029602
- Yang, Y., Qiu, Z., and Fan, H. (2024). “Close-in explosion performances and damage evaluation of bamboo fiber reinforced laminates,” *Thin-Walled Structures* 205, article ID 112461. DOI: 10.1016/j.tws.2024.112461
- Zhang, E., Chen, G., Zhu, W., Wang, C., and Yang, W. (2024). “Experimental investigation on withdrawal resistance performance of nails in southern pine,” *Engineering Structures* 306, article ID 117755. DOI: 10.1016/j.engstruct.2024.117755
- Zhang, H., Li, H., Dauletbek, A., Lorenzo, R., Corbi, I., and Corbi, O. (2023). “Research status of glued-in rods connections in wood structures,” *Journal of Building Engineering* 65, article ID 105782. DOI: 10.1016/j.job.2022.105782
- Zhao, J., Meng, Z., Jin, Z., Dong, C., Wu, Y., and Wei, Z. (2019). “Bending properties of bamboo scrimber with holes in different sizes and positions,” *Construction and Building Materials* 200, 209-217. DOI: 10.1016/j.conbuildmat.2018.12.076
- Zhong, Y., Wu, G., Ren, H., and Jiang, Z. (2017). “Bending properties evaluation of newly designed reinforced bamboo scrimber composite beams,” *Construction and Building Materials* 143, 61-70. DOI: 10.1016/j.conbuildmat.2017.03.052
- Zhu, W., Qiu, Z., Zhou, J., and Fan, H. (2022). “Size design and nonlinear stress-strain relationship of parallel bamboo strand lumbers in tension and compression,” *Engineering Failure Analysis* 140, article ID 106587. DOI: 10.1016/j.engfailanal.2022.106587

Article submitted: October 10, 2024; Peer review completed: December 9, 2024; Revised version received and accepted: December 12, 2024; Published: December 20, 2024.  
DOI: 10.15376/biores.20.1.1691-1702